Investigating OpenSim for Simulating Gait Restoration with a Knee Exoskeleton

Anish Behera[1], Samyak Kumar Mishra[1], Japteshwar Singh[1], Matthew Wong Sang[2], Jyotindra Narayan[3,4]
[1]*Department of Mechanical Engineering, Thapar Institute of Engineering and Technology, Patiala, Punjab, India*
[2]*Department of Bioengineering, Imperial College London, UK*
[3]*Department of Mechanical Engineering, Indian Institute of Technology Patna, Bihar, India*
[4]*Department of Computing, Imperial College London, UK*
banish860@gmail.com, msamyak1@gmail.com, japteshwarsingh01@gmail.com,
mwongsang@gmail.com, n.jyotindra@gmail.com

***Abstract*—Post-stroke gait abnormalities significantly reduce mobility, independence, and quality of life. This study presents a simulation-based evaluation of a unilateral thigh-and-shank knee exoskeleton modeled in OpenSim to assist gait correction in stroke survivors. Using subject-specific scaling, inverse kinematics, and dynamic simulations, joint kinematics of able-bodied, post-stroke, and exoskeleton-assisted individuals are analyzed. A proportional controller applied assistive torque at the knee joint to enhance gait alignment. Quantitative metrics are employed to assess performance, including range of motion analysis, RMS deviation, dynamic time warping, and Spearman's correlation. The exoskeleton achieved a notable 87.1% similarity in knee joint trajectories to healthy gait, improved Spearman correlation at the hip from 0.59 to 0.96, and enhanced joint coordination patterns. While knee correction was most effective, moderate improvements were observed at the ankle and partial correction at the hip. These results highlight the potential of targeted exoskeleton assistance and musculoskeletal simulation for advancing personalized stroke rehabilitation strategies.**

***Index Terms*—post-stroke gait, knee exoskeleton, OpenSim simulation, musculoskeletal modeling, joint coordination**

I. Introduction

An abnormal gait pattern is a frequent outcome of stroke, which results in compromised mobility, impaired balance, and chronic disability. Approximately 15 million people have strokes each year, and more than half have transient or permanent gait dysfunction [1]. An abnormal gait decreases the quality of life, enhances the risk of falling, and promotes dependency. Successful rehabilitation of the lower limbs is thus critical to achieving independence and mobility [1], [2]. Although useful, conventional rehabilitation methods such as body-weight-supported treadmill training and therapist-managed gait retraining tend to lack customizability, reproducibility, and long-term benefits. In recent years, robotic and exoskeleton-type gait rehabilitation devices have emerged. These devices provide repetitive, high-intensity, and user-autonomous training, crucial for neoplastic recovery after stroke [2], [3]. Research has indicated that robot-assisted gait training enhances spatiotemporal gait parameters, walking speed, and balance, especially when initiated early in the subacute stages of recovery [3], [4].

Most commercial systems, however, address a finite number of joints or do not have customized designs according to particular impairments. Mismatches between exoskeleton joints and anatomical landmarks can lead to elevated muscle stress or discomfort, as in the rectus femurs, during stiff-knee gait conditions [5]. Personalized exoskeleton settings and control approaches, like subject-specific hip-knee torque coordination, have been advocated to avoid such issues and support effective gait recovery [5], [6]. Musculoskeletal simulation and modeling on platforms like OpenSim is a robust alternative to expensive and time-consuming physical prototyping [7], [8]. Simulation-based investigations enable researchers to compare joint-level kinematics, torque demands, and muscle coordination across different assistive strategies. They also allow for a more in-depth investigation of the biomechanical effects of stroke, such as asymmetries in joint activation and prolonged muscle response [9].

Current developments in simulation platforms have made it possible to create patient-specific models that account for spasticity thresholds, neuromuscular deficits, and anatomical differences [5], [9]. Such models yield data-driven insights for exoskeleton design and prescription, and they present a route toward adaptive, user-driven rehabilitation solutions [8], [10]. Various modeling and experimental frameworks have been investigated in previous research, like the deployment of biomechanical simulation to compare lower limb support [11], creating a powered exoskeleton walking simulation model for spinal cord injury subjects, with a focus on gait mechanics and ground reaction forces [7] and concentrating on impairment-specific prescription through the incorporation of reflex thresholds to reduce spasticity in stiff-knee gait [5]. Although these studies have provided a helpful starting point, numerous studies limit themselves to a single joint or two, i.e., hip and knee, with the ankle frequently excluded [3], [6]. Some studies hardly focus on simulating targeted aid for the post-stroke population [12], [13]. Others restrict their simulations to perfect conditions or do not investigate actual patient variability in musculoskeletal responses [14].

This work assesses a unilateral thigh-and-shank-based exoskeleton designed in OpenSim to correct post-stroke gait abnormality. The exoskeleton supports only one leg, specifically correcting joint angles at the hip, knee, and ankle. The main goal is to see if the exoskeleton can assist post-stroke

kinematics in reaching able-bodied gait patterns. The rest of the paper's structure is as follows: Section II provides the validation dataset description; Section III details the methodology followed, such as scaling and inverse kinematics analysis; Section IV provides the results and discussion; and Section V concludes with findings and recommendations for future research.

II. Related Data and Processing

In this study, we utilize gait data from an open-access dataset [15] comprising 8 able-bodied subjects and 6 stroke survivors aged between 70 and 75 years. The stroke group consisted of participants with a variety of functional impairments resulting from both ischemic and hemorrhagic strokes. Data were collected at the Multidisciplinary Motor Centre Antwerp with a full-body motion capture system. Reflective markers (Fig. 1) were attached to anatomical landmarks according to the Plug-In Gait model to extract precise joint kinematics. The able-bodied subjects walked barefoot along a 12-meter walkway at self-selected speeds, whereas stroke survivors performed supervised trials to guarantee safety and unimpeded marker tracking. The dataset contains sagittal plane kinematic information for the hip, knee, and ankle joints. Each joint angle profile is sampled at 1001 time-normalized points during a complete gait cycle. Metadata accompanying each subject contains demographic and anthropometric information like age, sex, body weight, height, and leg length.

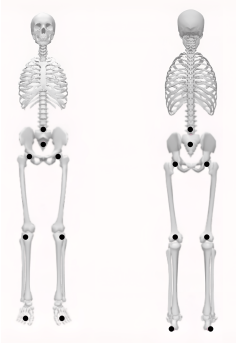

Fig. 1. Marker placement based on the Plug-In Gait model for full-body motion capture. Black dots indicate reflective markers positioned at anatomical landmarks.

III. Proposed Methodology

A. Subject-Specific Scaling and Inverse Kinematics for Able-Bodied and Post-Stroke Gait

To estimate joint kinematics for able-bodied and post-stroke subjects, the Gait2354 musculoskeletal model available in OpenSim was utilized due to its comprehensive representation of lower-limb and torso biomechanics and its compatibility with gait analysis workflows. The model was individually scaled for each subject using OpenSim's Scale Tool, which adjusts segment dimensions and mass properties to reflect subject-specific anthropometric parameters, including leg length, total height, and body mass, which were extracted

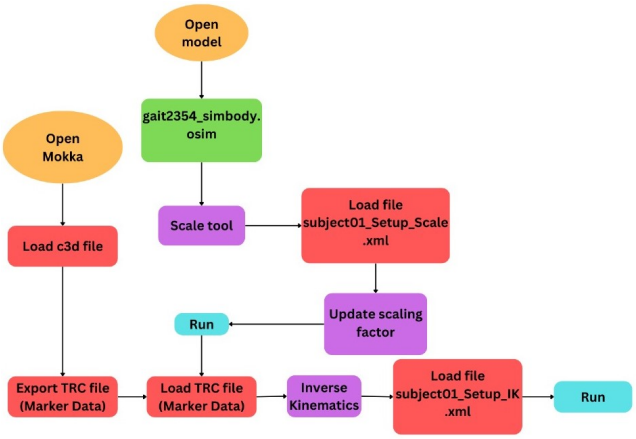

Fig. 2. Flowchart depicting the scaling and inverse kinematics using OpenSim.

from individualized data files (Fig. 2). In addition to automated scaling, manual refinement was performed to adjust the distribution of body mass, ensuring correct alignment of the center of mass. Key anatomical segments, namely, the pelvis, femur, tibia, talus, calcaneus, toes, and torso, were proportionally scaled based on geometric ratios to accommodate inter-subject anatomical variation. The scaling was based on subject-specific dimensions, e.g., leg length, and the scaling factors for every segment were computed with a standard formula [16]:

$$SF = \frac{1}{100} \times \left(100 - \left(\left(\frac{\mathrm{OL} - \mathrm{NL}}{\mathrm{OL}}\right) \times 100\right)\right) \quad (1)$$

where SF represents the scaling factor, and OL and NL indicate the old length and new length, respectively.

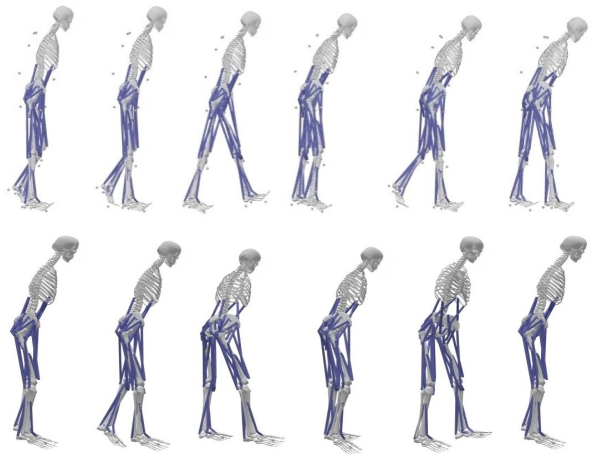

Fig. 3. Gait motion of an able-bodied subject (top) and a post-stroke subject (bottom) visualized in OpenSim.

Motion capture data were preprocessed using Mokka software to convert marker trajectories into .trc (tracking) files. These files were subsequently imported into OpenSim, where virtual markers on the model were mapped to corresponding anatomical landmarks through customized marker sets. This

mapping enabled accurate registration between experimental motion trajectories and the model's anatomical framework. Following the scaling and marker mapping steps, inverse kinematics (IK) analysis was modeled to derive ankle, knee, and hip joint angles throughout the gait cycle. The IK procedure was implemented via subject-specific configuration files, which minimized the squared error between experimental and model marker trajectories. Figure 3 visualizes the able-bodied and post-stroke gait motions after IK, respectively.

B. Integration of Knee-Assistive Exoskeleton and Joint Control Using OpenSim and Python

A custom knee-assistive exoskeleton was designed using Creo Parametric CAD software, comprising two primary components (Fig. 4): a thigh segment (460 mm) and a shank segment (370 mm). Each segment consisted of a rigid beam structure supported by two semi-circular clamps for stable fixation to the limb. Segments were interconnected via a pin joint at the knee to enable torque transmission during gait.

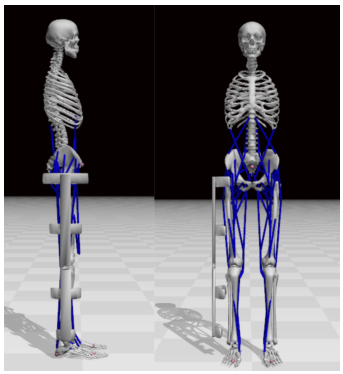

Fig. 4. Front and side views of the musculoskeletal model with a thigh-and-shank exoskeleton, visualized in OpenSim Creator. The exoskeleton components are attached to the lateral side of the right leg.

The exoskeleton model was imported into OpenSim and integrated into the Gait2354 model using OpenSim Creator (Fig. 5). The thigh and shank components of the exoskeleton were rigidly attached to the lateral side of the right leg using Pin joint connections with one linking the thigh component to the femur and the other linking the shank component to the tibia. Precise joint alignment was achieved using PhysicalOffsetFrame objects to ensure synchronized movement with the corresponding musculoskeletal segments. The thigh and shank components were physically connected at the knee via a shared Pin joint, allowing relative rotational movement. A coordinate actuator was applied to the joint to simulate active knee flexion, serving as the point of torque for assistive control. The actuator operated within a control range of -1.0 and 1.0, and an optimal force of 50.0. As shown in Fig. 5, A Prescribed Controller was used to govern the actuator, initialized with a placeholder control signal to validate functional integration within the model.

For forward dynamic simulation, a Python script leveraging the OpenSim was developed. The simulation was conducted on

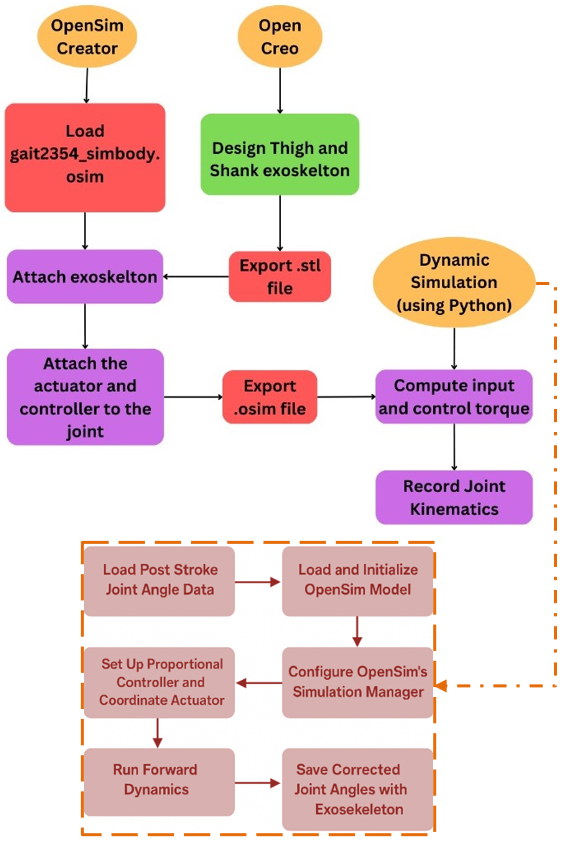

Fig. 5. Flowchart depicting the integration and simulation of exoskeleton (top) and forward dynamic simulation (bottom).

the model in which joint kinematics of a representative post-stroke subject served as reference trajectories. A proportional control strategy was implemented to compute the actuator input torque at a temporal resolution of 0.002 seconds. The control input was determined as a function of the instantaneous error between the simulated and reference knee angles, scaled by a proportional gain of 0.05. The control torque was applied to the Coordinate actuator, and the resulting motion was simulated using OpenSim's Manager Class. Due to differences in coordinate frame definitions between the IK-based and dynamically simulated models, especially in the presence of actuators and additional exoskeleton components, the resulting joint angles, particularly at the hip, may differ in sign convention from those generated via inverse kinematics. Therefore, to ensure valid comparisons across all three conditions, we opted to adjust the orientation of the able-bodied hip angle, so that it aligns with the orientation used in the dynamic simulations. The simulation parameters included a step size in the range of 0.00001 to 0.002 seconds, with an accuracy of 0.001. Joint kinematics at the hip, knee, and ankle were monitored and recorded for post-simulation analysis (Fig. 6) to assess the influence of the assistive exoskeleton on gait performance.

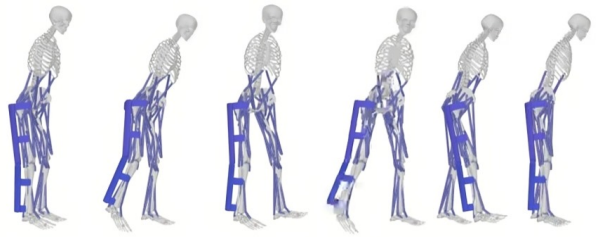

Fig. 6. Gait motion of an exoskeleton-assisted post-stroke subject in Opensim.

C. Performance Metrics

To evaluate the effectiveness of exoskeleton-assisted gait correction, multiple quantitative metrics were employed, including Shaded Gait with Range of Motion (ROM) comparison, Root Mean Square Deviation (RMSD), Dynamic Time Warping (DTW), Spearmen's rank correlation coefficient, and Cyclogram plots. Shaded Gait and Range of Motion (ROM) plots were employed to qualitatively assess the variability and overlap in joint trajectories across the gait cycle for able-bodied, post-stroke, and exoskeleton-assisted individuals. These mean $\pm$ standard deviation plots helped visualize consistency and deviations across joints. ROM values served as additional indicators of joint performance. To quantify joint-level correction, RMSD was calculated between exoskeleton-assisted and able-bodied trajectories, with a phase-wise breakdown across five key gait phases to identify when correction was most effective. Additionally, DTW was applied to evaluate time-series similarity between gait trajectories, computing distances between exoskeleton-assisted vs. able-bodied and post-stroke groups. Normalized DTW values were further used to estimate percentage similarity, offering a comprehensive understanding of how closely the exoskeleton-corrected gait aligned with healthy patterns.

$$\text{Similarity} = \frac{1}{100} \times \left(1 - \left(\frac{\text{DTW}_{PS/ES} - \text{DTW}_{AB/ES}}{\text{DTW}_{PS/ES}}\right)\right) \quad (2)$$

where PS, ES, and AB represent the post-stroke, exoskeleton-assisted, and able-bodied gait trajectories.

Spearman's rank correlation coefficient was employed to compute the relationship between joint hip, knee, ankle angle trajectories of able-bodied and post-stroke subjects, as well as between able-bodied and exoskeleton-assisted post-stroke subjects. Cyclogram plots were used to offering a representation of inter-joint coordination patterns throughout the gait cycle. These plots were particularly useful for comparing complex movement patterns between different conditions such as able-bodied, post-stroke and exoskeleton-assisted gait.

IV. Results and Discussions

This study aimed to assess how effectively a knee exoskeleton supports walking rehabilitation in post-stroke survivors by comparing movement patterns across three groups: able-bodied with 8 subjects, post-stroke with 6 subjects, and 6 post-stroke subjects assisted with the exoskeleton. A total of 6 exoskeleton-assisted simulations were conducted, one for each post-stroke subject, and compared to their own pre-assist gait and age-matched able-bodied references. All joint trajectories were time-normalized to 1001 points per gait cycle to enable uniform and computationally simple comparison across subjects. We analyzed joint movements using various approaches: Shaded gait graphs and ROM values for tracking different joint motions through walking cycles, RMSD to quantify differences in knee angles, DTW, Spearmen's rank correlation coefficient, and Cyclogram plot to evaluate the effectiveness of the exoskeleton correction.

Table I presents the ROM values for the hip, knee, and ankle joints as calculated by OpenSim simulations. For the hip joint, the able-bodied subjects exhibited a flexion-extension range of -33° to 0.03°, while the post-stroke subjects showed a significantly reduced range (-18.27° to -4.26°), indicating restricted motion in pathological gait. The exoskeleton-assisted post-stroke subjects demonstrated an altered hip motion pattern (9.52° to -5.47°), suggesting compensatory changes likely induced by exoskeleton assistance. The able-bodied subjects had a ROM of -1.59° to 35.81° for the knee joint, representing normal knee extension and flexion. The post-stroke subject exhibited an excessive knee extension (22.84°) with reduced flexion (30.35°), reflecting the characteristic stiff knee gait in stroke survivors. In contrast, the exoskeleton-assisted subjects showed improved knee dynamics (-3.51° to 27.85°), demonstrating more balanced flexion-extension patterns, likely facilitated by the exoskeleton. For the ankle joint, the able-bodied subjects displayed a plantarflexion-dorsiflexion range of -31.93° to -4°, characteristic of healthy push-off and foot clearance. The post-stroke subjects had limited plantarflexion (-17.43°) and slightly reduced dorsiflexion (-6.89°), indicative of foot drop and impaired propulsion. In the exoskeleton-assisted subjects, while dorsiflexion further decreased (-9.20°), plantarflexion significantly increased (-41.87°), suggesting that exoskeleton assistance may have enhanced push-off mechanics but altered ankle dorsiflexion control.

Fig. 7 presents a shaded graph of each joint angle across one gait cycle for all three groups. The plots reveal significant improvements in both the magnitude and the shape of the knee and ankle curves in Group C compared to Group B. Specifically, the corrected gait profiles for the knee and ankle in Group C not only exhibit joint angle values closer to those of healthy adults but also follow a similar overall pattern. In contrast, the hip joint shows only slight improvements in both curve shape and absolute angle values. Overall, the shaded curves for Group C align more closely with the patterns observed in Group A than those in Group B, highlighting the effectiveness of the exoskeleton in restoring gait mechanics.

The bar graph (Fig. 8) illustrates the phase-wise comparison of gait deviations between post-stroke and exoskeleton-assisted subjects relative to able-bodied subjects. The phase-wise analysis indicates that the knee exoskeleton significantly enhances gait kinematics in post-stroke individuals, especially by reducing deviations at the knee and ankle during the stance

TABLE I
RANGE OF MOTION FROM OPENSIM SIMULATIONS

Group/Joint	Hip		Knee		Ankle	
	Ext	Flex	Ext	Flex	Plantar	Dorsi
Able-Bodied	0.03 ± 4	-33 ± 3.99	-1.59 ± 4.09	35.81 ± 6.61	-31.93 ± 5.22	-4 ± 3.71
Post-Stroke	-4.26 ± 2.19	22.84 ± 10.10	3.63 ± 2.09	30.35 ± 9.61	-17.43 ± 6.89	-6.89 ± 2.79
Exoskeleton Assisted	-5.47 ± 6.22	9.52 ± 4.15	-3.51 ± 4.40	27.85 ± 6.46	-41.87 ± 8.62	-9.20 ± 8.65

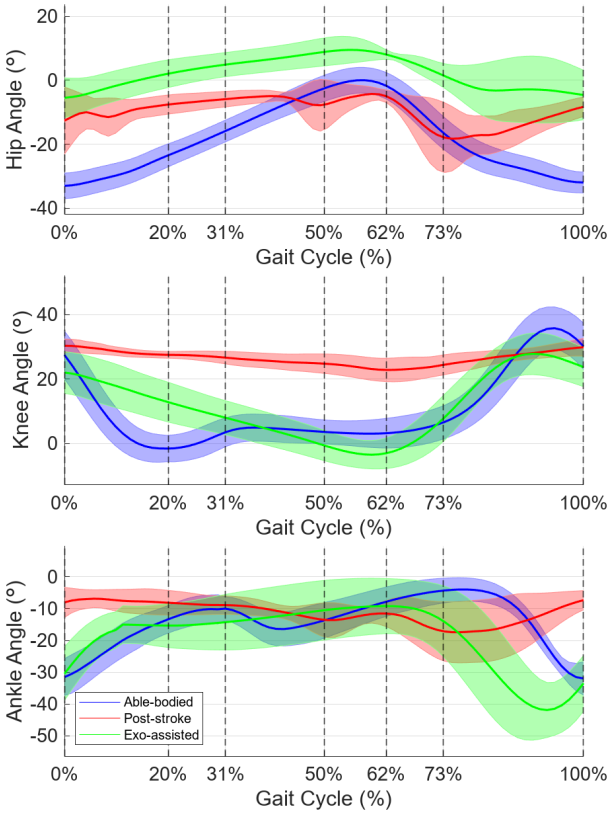

Fig. 7. Comparison of the hip, knee, and ankle angles over the gait cycle for able-bodied (blue), Post-stroke (red), and Exoskeleton-assisted (green). In the figure, 0-20%: Loading response, 20-31%: Mid-stance, 31-50%: Terminal Stance, 50-62%: Pre-Swing, 62-73%: Initial Swing, 73-100: Terminal Swing.

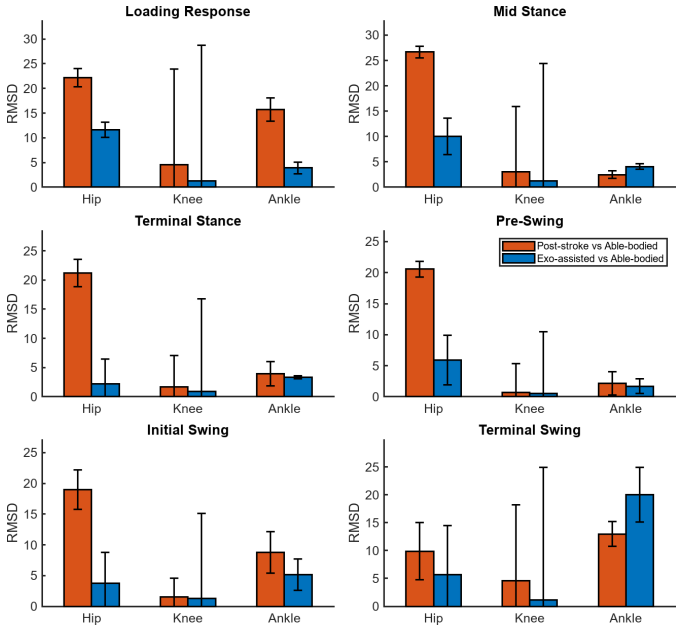

Fig. 8. RMSD value of joint angle deviations between post-stroke and exoskeleton-assisted gait relative to able-bodied gait across gait sub-phases.

and swing phases. Despite the hip alignment showing moderate improvement, it remains the most challenging joint to correct, reinforcing the need for enhanced control strategies or multi-joint actuation. Overall, the exoskeleton offers effective support for weight acceptance, push-off, and swing initiation.

To evaluate the similarity between the gait patterns of different subject groups, DTW was applied to compare joint angle trajectories across the gait cycle. The exoskeleton achieved a remarkable 87.1% similarity for the knee joint, closely aligning the corrected gait with the healthy pattern. This strong improvement can be attributed to the placement of the actuator directly at the knee joint, enabling more targeted and effective assistance. The ankle joint showed 63.9% similarity, indicating substantial but lesser correction, while the hip joint exhibited only 53.4% similarity, suggesting that the corrected gait remained less aligned with healthy movement.

While DTW analysis indicated that the exoskeleton provided the most significant shape correction at the knee joint, with moderate alignment at the ankle and marginal improvement at the hip, Spearman's correlation Fig. 9 presented a contrasting outcome—highlighting the highest improvement in trend consistency at the hip joint, where correlation increased markedly from 0.59 to 0.96. Contrariwise, the knee had a moderate rise (0.38 to 0.64), and the ankle shifted from a negative correlation (-0.75) to a weak positive (0.35). These findings suggest that while the exoskeleton is most effective in restoring the overall shape and timing of motion at the knee joint, it more substantially enhances the temporal coordination and directional consistency of hip movements. This contrast observation underscores the importance of using both metrics for a holistic understanding of gait correction—DTW similarity for evaluating geometric alignment and Spearman's correlation for unlocking consistent joint behavior.

The cyclogram plots (Fig. 10) reveal clear improvements in joint coordination with exoskeleton assistance. Compared to the post-stroke gait, which shows restricted and irregular joint trajectories, the exoskeleton-assisted curves are broader and more continuous, indicating enhanced inter-joint coordination. Notably, the hip–knee and knee–ankle plots demonstrate a strong shift toward healthy patterns, while the ankle–hip plot

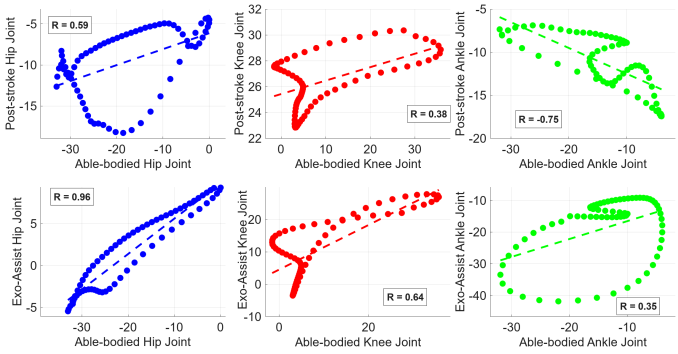

Fig. 9. Spearman correlation plots comparing joint angle trajectories of able-bodied individuals with those of post-stroke individuals (left) and exoskeleton-assisted post-stroke individuals (right) for the hip (blue), knee (red), and ankle (green) joints.

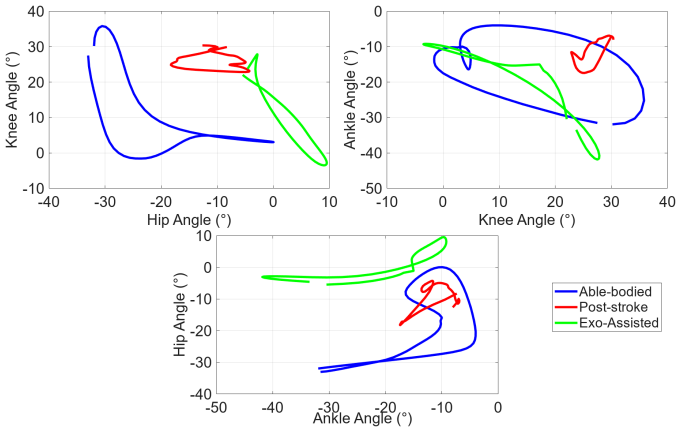

Fig. 10. Joint coordination patterns across the gait cycle for able-bodied (blue), post-stroke (red), and exoskeleton-assisted (green) subjects.

shows partial improvement, reflecting ongoing limitations in ankle control. Overall, the exoskeleton aids in restoring more natural gait dynamics, particularly at the hip and knee joints.

In summary, among the various performance metrics employed in this study, ROM and cyclogram-based inter-joint coordination emerge as the most clinically interpretable and relevant for rehabilitation assessment. While DTW and Spearman's correlation offer valuable quantitative insights into trajectory similarity and movement trends, ROM provides a direct measure of functional recovery, and cyclogram plots offer a comprehensive view of joint coordination, which is a key indicator in evaluating the effectiveness of multi-joint rehabilitation strategies.

V. Conclusions

This study demonstrated the effectiveness of a unilateral thigh-and-shank knee exoskeleton, modeled in OpenSim, in improving knee kinematics and partially correcting hip and ankle motion in post-stroke gait. By leveraging an open-source, cost-free simulation framework, we provided a practical approach for early-stage exoskeleton evaluation. While time-normalized trajectories enabled simplified control, they may not fully capture subject-specific gait phase variation. Future work will integrate phase-aware alignment with advanced control schemes, validate findings against empirical exoskeleton trials, and explore bilateral assistance and design variations. Further integrating muscle force in simulations would provide a deeper understanding of rehabilitation efficacy.

References

[1] B. Kalita, J. Narayan, and S. K. Dwivedy, "Development of active lower limb robotic-based orthosis and exoskeleton devices: a systematic review," *International Journal of Social Robotics*, vol. 13, pp. 775–793, 2021.

[2] A. Gupta, N. B. Prakash, P. Honavar, M. Khanna, S. Ramakrishnan *et al.*, "Robotic exoskeleton-assisted gait training in patients with motor incomplete myelopathy," *Journal of the International Society of Physical and Rehabilitation Medicine*, vol. 7, no. 3, pp. 99–104, 2024.

[3] L. Vianello, C. Lhoste, E. B. Küçüktabak, M. Short, L. Hargrove, and J. L. Pons, "Deep-learning control of lower-limb exoskeletons via simplified therapist input," *arXiv preprint arXiv:2412.07959*, 2024.

[4] J. Narayan and S. K. Dwivedy, "Adaptive control of a pediatric gait exoskeleton: Integrating rbf neural network with non-singular fast terminal sliding mode scheme," in *2024 10th International Conference on Control, Decision and Information Technologies (CoDIT)*. IEEE, 2024, pp. 922–927.

[5] T. Akbas and J. Sulzer, "Musculoskeletal simulation framework for impairment-based exoskeletal assistance post-stroke," in *2019 IEEE 16th International Conference on Rehabilitation Robotics (ICORR)*. IEEE, 2019, pp. 1185–1190.

[6] Q. Zhang, X. Tu, J. Si, M. D. Lewek, and H. Huang, "A robotic assistance personalization control approach of hip exoskeletons for gait symmetry improvement," in *2023 IEEE/RSJ International Conference on Intelligent Robots and Systems (IROS)*. IEEE, 2023, pp. 6125–6132.

[7] B. N. Fournier, E. D. Lemaire, A. J. Smith, and M. Doumit, "Modeling and simulation of a lower extremity powered exoskeleton," *IEEE transactions on neural systems and rehabilitation engineering*, vol. 26, no. 8, pp. 1596–1603, 2018.

[8] D. Coll Pujals, "Simulation of the assistance of an exoskeleton on lower limbs joints using opensim," Master's thesis, Universitat Politècnica de Catalunya, 2017.

[9] G. Giarmatzis, S. Fotiadou, E. Giannakou, C. Kokkotis, T. Fanaradelli, S. Kordosi, K. Vadikolias, and N. Aggelousis, "Understanding post-stroke movement by means of motion capture and musculoskeletal modeling: a scoping review of methods and practices," *BioMed*, vol. 2, no. 4, pp. 409–421, 2022.

[10] A. Nandy and P. Chakraborty, "A study on human gait dynamics: modeling and simulations on opensim platform," *Multimedia Tools and Applications*, vol. 76, pp. 21 365–21 400, 2017.

[11] Y. Wu, A. Zhu, H. Shen, Z. Shen, X. Zhang, and G. Cao, "Biomechanical simulation analysis of human lower limbs assisted by exoskeleton," in *2019 16th International Conference on Ubiquitous Robots (UR)*. IEEE, 2019, pp. 765–770.

[12] D. Mosconi, Y. Moreno, and A. Siqueira, "Exploring human–exoskeleton interaction dynamics: An in-depth analysis of knee flexion–extension performance across varied robot assistance–resistance configurations," *Sensors*, vol. 24, no. 8, p. 2645, 2024.

[13] D. M. Mohan, A. H. Khandoker, S. A. Wasti, S. Ismail Ibrahim Ismail Alali, H. F. Jelinek, and K. Khalaf, "Assessment methods of post-stroke gait: A scoping review of technology-driven approaches to gait characterization and analysis," *Frontiers in Neurology*, vol. 12, p. 650024, 2021.

[14] B. A. Killen, A. Falisse, F. De Groote, and I. Jonkers, "In silico-enhanced treatment and rehabilitation planning for patients with musculoskeletal disorders: can musculoskeletal modelling and dynamic simulations really impact current clinical practice?" *Applied Sciences*, vol. 10, no. 20, p. 7255, 2020.

[15] T. Van Criekinge, W. Saeys, S. Truijen, L. Vereeck, L. H. Sloot, and A. Hallemans, "A full-body motion capture gait dataset of 138 able-bodied adults across the life span and 50 stroke survivors," *Scientific data*, vol. 10, no. 1, p. 852, 2023.

[16] S. Younis, A. Bishnoi, J. Narayan, and R. Mio, "Impact of contralateral hemiplegia on lower limb joint kinematics and dynamics: A musculoskeletal modeling approach," *Biomechanics*, vol. 4, no. 4, pp. 784–804, 2024.